Direct Manufacturing of Functional Structures on 3D microscale surfaces by Laser Dynamic Forming

Huang Gao, Gary J.Cheng

Birck Nanotechnology Center and School of Industrial Engineering,
Purdue University, West Lafayette, IN 47906
email: gjcheng@purdue.edu

ABSTRACT

This paper demonstrates a scalable and fast-shaping top-down integration technique, Laser Dynamic Forming (LDF), capable of manufacturing 3D functional structures conformal to micro-to-mesoscale curvilinear features on various substrates by the laser-induced shockwave. The functional devices in this study, temperature sensors, preserved their electrical resistance and temperature coefficient of resistance (TCR) after selectively laser forming on metallic interconnections. The ductile interconnections inherit 3D microscale structures on various substrates and experience significant plastic deformations without excessive necking and fracture. It was realized by the polymeric encapsulation of functional materials and the shockwave controlled by laser pulse intensity. It was revealed in experiments and analytical solutions that the encapsulation layer (parylene-C) absorbs most of shockwave energy by large thickness reduction and extends the formability of ductile interconnections by high-quality deposition and bonding. Comparatively, the thickness of ductile functional materials was reduced very limitedly and uniformly along the 3D microfeatures by low and moderate laser intensities. The manufacturability of functional structures is determined by the applied laser intensity, as well as the size and aspect ratio of 3D microfeatures.

Keywords: direct manufacturing, functional materials, 3D microscale surfaces, laser dynamic forming

1 INTRODUCTION

The growing applications of micro-to-mesoscale electromechanical systems (MEMS), such as artificial human implant, sensory skins for robotics [1], flexible solar cells [2] and memory transistors [3], call for the packaging and integration of heterogeneous materials and components with three-dimensional (3D) surfaces, which are usually incompatible in a monolithic fabrication approach. Though current lithography-based technologies are very successful in fabricating high-performance, rigid and brittle devices on planar semiconductor substrates, there exists significant challenges in the fabrication and assembly of these devices on irregular and curvilinear 3D surfaces without compromise in performance and efficiency. Various techniques have been developed to manufacture 3D patterned microscale structures of both inorganic and polymeric materials, such as 3D lithographic patterning [4-5], guided self-assembly [6-7], inkjet printing [8] and soft-lithographic-based fabrication [9]. However, these methods are time consuming and limited in throughput. To address these limitations, direct templating techniques have been developed to replicate or transfer 3D patterns from master template to relatively softer materials, such as nanoimprint lithography[10] and detachment lithography [11-12]. The multistage transfer, the selective bonding and the specifically designed interconnection bridges, result in low yield and limit its mass production capabilities. Therefore, there is an urgent need to develop scalable and fast-shaping techniques that can manufacture MEMS devices on curvilinear 3D surfaces efficiently, with a wide spectrum of functional materials. This study will investigate an transformative means to directly manufacture MEMS on 3D surface by a newly developed forming process, namely laser dynamic forming (LDF) [13]. On the other hand, the compressive shockwave pressure could introduce plastic strain and microstructural defects to functional materials. To preserve the functionality during LDF, functional materials are encapsulated by elastomeric layers, which absorb most of the shock energy and minimize the defects in functional materials. The laser pulse energy and the shockwave pressure are also controlled in a range to achieve the deformation faithful to 3D surfaces without degrading the performance of the structures.

2 RESULTS AND ANALYSIS

Fig. 1 (a) illustrates the process scheme of patterned LDF of functional structures on 3D microscale surfaces. The laser pulse transmits through confining media, such as glass slide, and irradiates ablation layer into plasma plume. Restricted by confinement, the plasma turns into a shockwave propagating through functional materials which acquire microscale deformations conformal to the underlying 3D surfaces. The functional materials are also bonded with 3D surfaces by uniformly coated adhesive as the dynamic deformation completes in a few nanoseconds. Compared to multiple-stage transfer technologies, this non-contact method eliminates the need to fabricate inverted molds for surface replication, which could be costly and unpractical at the microscale. As the shockwave pressure is primarily determined by the applied laser intensity [14], the laser pulse energy could be programmed to keep shockwave pressure under control for different functional materials and substrates in order to preserve the proper function of fabricated devices. This technology also provides much

flexibility and selectivity in assembly location and area since the scanning speed, focal plane and coordinates of laser beam are readily adjusted by optical configurations and the motorized X-Y-Z translation stage. Fig. 1 (b) shows another way to control plastic deformation of functional materials by the patterned 3D surface to allow different regions (fragile devices and ductile connections) to experience different deformations during LDF. It is expected that metallic connections aligned to wavy regions will have moderate plastic deformation, while the devices aligned with flat regions will have minimal plastic deformation.

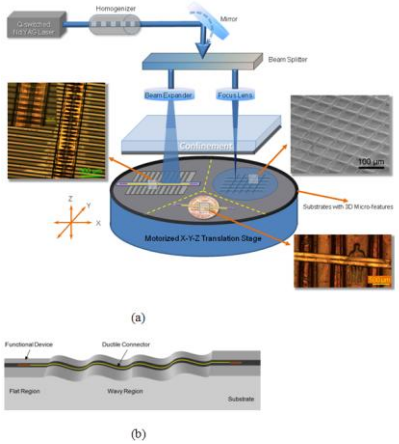

Fig. 1. (a) Schematic setup of laser dynamic forming process to manufacture functional structure on 3D microscale surface. (b) Controlled fabrication of laminated structure on 3D patterned surface.

Fig. 1 (a) also shows the conformal assembly of functional devices and materials on 3D surfaces of different materials. A temperature sensor acquired the deformation defined by regular micropatterns on Si wafer. The ductile wire connection was selectively deformed above micropatterns while the functional sensing part was aligned with even regions to experience minimal plastic deformation. The laser intensity was controlled to avoid excessive compression and necking of functional material. The sensor resistivity changed from 1.18KΩ to 1.19KΩ after LDF and TCR was kept unchanged at approximately 0.11%/℃. It directly proves that LDF is a feasible solution to produce 3D microscale structures and preserve the proper functioning of fabricated devices by controlled plastic deformation. The regular micropatterns on Si wafer were replaced by mesoscale patterns on coins to demonstrate the scalability of LDF. Another temperature sensor was deformed compliantly on mesoscale pillars of one cent. The sensor resistivity changed from 1.35KΩ to 1.42KΩ after LDF and TCR was unchanged at approximately 0.12%/℃, which indicated that the deformation was controlled to prevent the fracture of functional layer. The scalability of LDF is realized by increasing laser beam size and pulse energy to achieve the same laser intensity over larger area.

Fig. 2 illustrates the effects of laser intensity on functional materials. As-received 5um thick laminated thin film was deformed on top of TEM mesh grid (G1000HS) by the increased laser intensities. The thickness changes of Au and parylene layer at the top (Section A) and corner (Section B) of grid bar were measured in FIB/SEM and normalized in Fig. 2. In general, the thicknesses of all materials decreased with laser intensities. But there are some remarkable differences between Au and parylene in deformation behaviors. While there was significant thickness reduction in parylene throughout all the laser intensities, Au layer only experienced a small amount of attenuation by low and moderate laser intensities. At high laser intensities, the excessive shockwave energy induced the delamination between Au and parylene, which again lead to the drastic necking and fracture of Au layer. The variances of Au and parylene thickness also increased at high laser intensities as the location and magnitude of necking initiation became more unpredictable. When the shockwave propagates through laminated materials, the steeply rising shockwave front induces viscoelastic compression and acceleration to material velocity instantaneously, followed by a second stage of slower viscoplastic compression and viscous relaxation. Compared with functional materials, parylene is more compressible because in semicrystalline polymers, densities of amorphous organic polymers are typically lower than that of crystalline regions of ordered lamellae. The shear stress in the shock front exceeds the strength of parylene, so that its bulk and shear moduli are reduced and it becomes more compressible. In the second viscous relaxation stage, shear relaxation and volume relaxation coexist when polymer chains go over barriers to pack tighter and result in plastic deformations [15]. After shockwave unloading, since some of polymer chains remain trapped in a partially densified state, only part of polymer volume recovers. That is, the majority of shockwave energy is converted to strain energy stored in the parylene, which will also be characterized in the finite element method (FEM). As shock compression by an instantaneous front is an irreversible adiabatic process with associated entropy increase, the laser intensity must be controlled to minimize microstructural defects and avoid voids, delamination and excessive necking in functional materials.

Fig. 2 (b) and (c) revealed the contrary behaviors in thickness change of the top and bottom parylene layer at the top and corner of grid bar due to different local deformation behaviors. At the top of grid bar (Section A), the materials underwent the shockwave compression primarily. The top layer had more thickness reduction than the bottom layer since the shockwave was at its peak on the top surface and decayed through the propagation direction. On the other hand, at the bar corner (Section B), the materials were not only compressed, but also bended and stretched more severely when the deformation curvature decreased near the grid bar. That is why the bottom layer thickness was more reduced than the top layer at Section B.

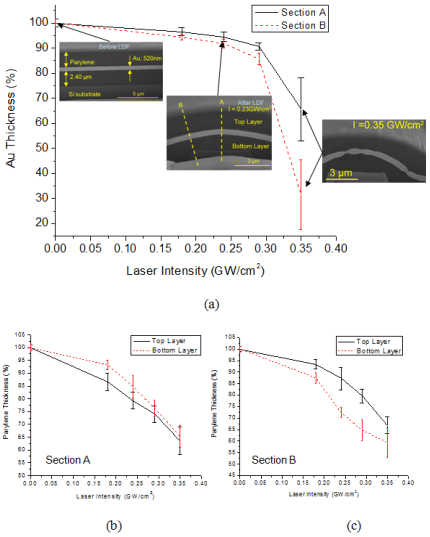

Fig. 2 (a) The thickness reduction of Au layer at the top and corner of grid bar, with the cross sections of laminated thin film before and after LDF; (b-c) The thickness reduction of top and bottom parylene layer at two sections.

Fig. 3 shows that the manufacturability of functional structures not only depends on the applied laser intensities, but also the size and aspect ratio of microscale features. It was observed that when the thickness of Slim-Bar TEM Grids, i.e. the height of grid bar, increased from 3.6um to 6.7um, Au layer in the laminated film experienced excessive necking at the top or corner of grid bar due to localized intensive stretching and bending, which could possibly lead to functional degradation or loss.

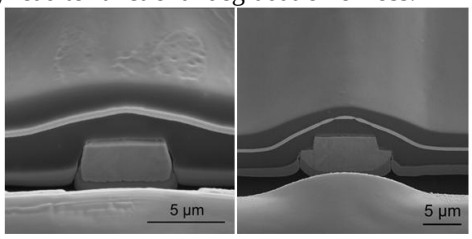

Fig. 3 The FIB/SEM images of cross sections of laminated thin film deformed on G1000HS Mesh Grid (a) and G400HS Mesh Grid (b). The sample was tilted at 52o in (a) and 40o in (b).

In Fig. 3, the total plastic strain in Au layer reached more than 10% by rough analytic calculations. It has been reported that if metallic connections are freestanding, their rupture strain is close to a very small strain needed to nucleate microcrack due to low hardening capability and small thickness-to-length ratio, resulting in the local elongation proportionate to metallic film thickness [16-17]. On the other hand, when metallic connections are well deposited on a polymer substrate, they could sustain strain up to a few tens of percent without appreciable cracks since the localized necking could be suppressed by the adherent substrate [18-21]. In this study, three mechanisms coexist to achieve uniform and significant plastic strain in functional layer. First, the functional layer was encapsulated by two parylene layers. The parylene layer not only allows functional material to sustain large plastic strain, but also provides compliant media between functional layer and sharp microfeatures to mitigate the localized intensive deformation. More importantly, the permanent plastic deformation of parylene layer absorbs most of laser-induced shockwave energy. Secondly, the through-thickness compressive shockwave suppresses the debonding between parylene and Au layer so as to reduce the localized necking. Lastly, another thin Cr layer was added before Au deposition to improve the bonding strength of Au on parylene layer.

The experimental conditions in Fig. 3(a) were incorporated in the analysis, with the results of Von Mises and total plastic strain distribution in the deformed structure in Fig. 4. It shows that the intensive stress and strain concentrate mostly in parylene layer, other than functional connection layer, the locations of which are top and corner of microgrid. The thickness of parylene layer could be customized to provide maximum protection and prevent functional layer from crack and failure. Along the through-thickness direction, such as section A, the stress distribution is discontinuous because the heterogeneous materials, Au and parylene, are different in the dynamic constitutive behavior while they are connected by tie constraint to avoid relative motions in the model. This stress discontinuity, as illustrated in Fig. 4 (c), tends to increase with the applied laser intensity, i.e. the shockwave energy. In the other way, it also represents the shear stress along the interface between Au and parylene layer. When the shear stress exceeds the bonding strength of Au layer, the delamination occurs and triggers the premature fracture of Au layer. It was also observed in experiments that under appropriate laser conditions, there was only very mild thickness reduction in Au layer while parylene thickness was reduced significantly. After dynamic deformation, the shockwave energy is primarily converted and stored as total strain energy in the materials. Assuming the volume of each material is kept constant, it reveals that the about 97% of total strain energy is stored in parylene and the average density of total strain energy in Au layer is only approximately 75% of that in parylene layer. The lower level of strain energy density in functional layer helps to preserve the functions in the long run and future transfer the deformed functional structures.

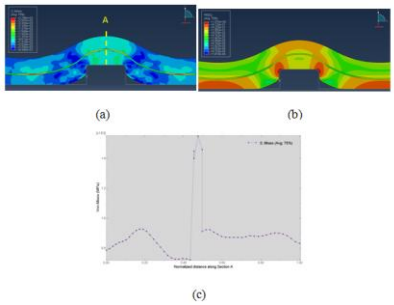

Fig. 4 The spatial distribution of plastic stress (a) and strain (b) in the deformed functional structure. (c): the stress discontinuity along section A in (a) by different laser intensities.

3 EXPERIMENTAL METHODS

A. Various substrates with 3D microscale patterns

The microscale patterns have been proved to be effective in changing the biocompatibility and hydrophobicity, light absorption and reflection. In this study, regular and irregular 3D microscale patterns were provided by three substrates of materials widely used in MEMS: Si wafer, polycarbonate (PC) and metals. One way to introduce large areas of micropatterns to Si wafer is photolithography and etching. Another way was to ultilize a series of copper SPI Slim-Bar® TEM Grids, Polycarbonate is widely used in micro-optics due to good transparency in the visible wavelengths, high optical absorbance in the deep-UV wavelength band, and thermal stability. The PC microlens in use consists of an array of concave pyramids with a side length of 80 μm and a height of 44 μm. Coins was also used to provid 3D irregular micropatterns on metallic surfaces. A thin photoresist layer, PMMA A4 or SU-8 2002 (Microchem Corp.), was spin-coated on these substrates or laminated thin films to act as an adhesion promoter in the assembly.

B. Laminated functional materials and devices

One of the keys to fabricate functional structures on 3D surfaces is to encapsulate them in an elastomeric material. Parylene-C is chosen to provide electrical insulation, moisture and chemical isolation, mechanical protection, enhanced lubricity, and surface consolidation to avert flaking or dusting. The functional materials include brittle materials in the sensor devices, such as SiO2, ZnO and polysilicon, and ductile materials in the wiring connections, such as Au/Cr. Since ductile materials in the wiring connections experience more complicated plastic deformations, another category of sample, parylene laminated thin film, was fabricated in order to investigate deformation characteristics of ductile connections under various conditions of laser intensities and microscale features. The laminated thin film included a thin metallic layer (Cr/Au) sandwiched by two layers of parylene.

C. Microstructure characterization in SEM/FIB

During LDF, the encapsulation layer, parylene, is expected to absorb most of the shockwave energy to protect functional materials from excessive deformation and fracture. In this study, the functional structures were characterized along the FIB-fabricated cross section to verify this assumption. The samples were tilted to 52◦ so that the gallium ion beam was perpendicular to the sample surface to prepare the cross section.

D. Characterization of functional structures

Functional device of temperature sensor was a resistor (Ti/Pt) which resistance varies with temperature. To experimentally demonstrate the proper working of the functional structure, the electrical resistance (at room temperature 23 ℃) and temperature coefficient of resistance (TCR) was measured before and after the laser forming. The measurement was operated on a probe station (The Micromanipulator Co., Inc.) connected with Agilent 4155C Semiconductor Parameter Analyzer. The initial resistance was obtained from room temperature to 83 ℃ with increment of 10 ℃.

4. CONCLUSIONS

Laser Dynamic Forming has been demonstrated to be a flexible and scalable top-down integration technology capable of manufacturing 3D microscale functional structures on those substrates commonly used in MEMS, without the compromise of device functional degradation. It was verified in terms of the morphologies and functions of functional devices and laminated thin films. The effects of these processing conditions have been characterized quantitatively by experimental observations and finite element analysis. The manufacturability is limited by the size and aspect ratio of inherited microscale features, which could be improved by optimized encapsulation layer.

REFERENCES

[1] Yang, Y.J., et al., Inter. J. of Advanced Manufacturing Technology, 2010. 46(9-12): p. 945-956.
[2] Na, S.I., et al., Adv. Materials, 2008. 20(21): p. 4061.
[3] Sekitani, T., et al., Science, 2009, 326(5959): p. 1516.
[4] Mehra, A., et al., Journal of Micro-electro-mechanical Systems, 2000. 9(4): p. 517-527.
[5] Yoon, Y.K. el at., Journal of Microelectromechanical Systems, 2006. 15(5): p. 1121-1130.
[6] Mastrangeli, M., et al., Journal of Micromechanics and Microengineering, 2009. 19(8).
[7] Gracias, D.H., et al., Advanced Materials, 2008. 20(24): p. 4760.
[8] Xu, T., et al., Tissue Engineering Part A, 2008. 14(5): p. 869-870.
[9] Whitesides, G.M., et al., Langmuir, 1999. 15(3): p. 826-836.
[10] Schift, H., Journal of Vacuum Science & Technology B, 2008. 26(2): p. 458-480.
[11] Yeom, J. and M.A. Shannon, Advanced Functional Materials, 2010. 20(2): p. 289-295.
[12] Ha, J.S., et al., Small, 2009. 5(23): p. 2703-2709.
[13] Gao, H. and G.J. Cheng, J. of Microelectromechanical Systems, 2010. 19(2): p. 273-281.
[14] Fabbro, R., et al., J. Applied Physics, 1990, 68(2): p. 775-784.
[15] Kim, H., S.A. Hambir, and D.D. Dlott, Journal of Physical Chemistry B, 2000. 104(17): p. 4239-4252.
[16] Huang, H.B. and F. Spaepen, Acta Materialia, 2000. 48(12): p. 3261-3269.
[17] Espinosa, H.D., B.C. Prorok, and M. Fischer, J. of the Mechanics and Physics of Solids, 2003. 51(1): p. 47.
[18] Lu, N.S., et al., Applied Physics Letters, 2007. 91(22).
[19] Niu, R.M., et al., Appl. Phy. Letters, 2007. 90(16).
[20] Akogwu, O., et al., J.of Appl. Physics, 2010. 108(12).
[21] Lu, N.S., Z.G. Suo, and J.J. Vlassak, Acta Materialia, 2010. 58(5): p. 1679-1687.